Experimental Verification of Dimensional Analysis Results on Flow Distribution and Pressure Drop for Disc-Type Windings in OD Cooling Modes

Xiang Zhang, Muhammad Daghrah, Zhongdong Wang, *Member, IEEE*, Qiang Liu, *Member, IEEE*, Paul Jarman, and Massimo Negro

***Abstract*—Oil-flow distribution in the winding has a direct impact on cooling performance. In addition, static pressure drop over the winding determines oil split among windings connected hydraulically in parallel. In this paper, experimental verifications are provided to support computational fluid dynamics (CFD) simulations for disc-type windings in oil-forced and directed (OD) cooling modes. Oil-flow distribution in and pressure drop over disc-type winding models are measured using a particle image velocimetry system and a differential pressure instrument, respectively. Dimensional analysis is adopted to analyze the relationship between flow distribution, or pressure drop, and the controlling parameters. CFD parametric sweeps of the dimensionless parameters obtained from the dimensional analysis are conducted and the CFD results are then correlated with the dimensionless parameters. The comparisons between measured results and corresponding results obtained from the correlations demonstrate constant consistency, proving the validity of both the method of dimensional analysis and the correlations. Finally, comparisons of experimental results from isothermal and nonisothermal conditions in OD cooling modes are executed, which show that the isothermal conclusions can be extended to nonisothermal cases because the effects of buoyancy force and hot-streak dynamics prove to be negligible.**

***Index Terms*—CFD, dimensional analysis, disc-type winding, flow distribution, OD, PIV, pressure drop, transformer.**

NOMENCLATURE

A	Cross sectional area of the vertical duct (m^2).
C_{pd}	Pressure drop coefficient over the winding model.
D_h	Hydraulic diameter (m) ($4A/P$).
H_{plate}	Plate vertical height (m).
H_{duct}	Horizontal duct height (m).
Gr	The Grashof number ($g\beta_T(T_{out}-T_{in})D_h^3/\nu^2$).
lpm	liters per minute.
n_1	Number of passes in the winding model.
n_2	Number of discs per pass.
P	Perimeter of the vertical duct (m).
P_{fi}	Volumetric flow proportion in horizontal duct i.
ΔP	Static pressure drop (Pa).
Re	The Reynolds number ($\rho \cdot \bar{v}_{in} \cdot D_h/\mu$).
Ri	The Richardson number (Gr/Re^2).
T	Temperature in Kelvin (K).
T_{in}	Temperature at pass 3 inlet in Kelvin (K).
T_{out}	Temperature at pass 3 outlet in Kelvin (K).
$\overline{v_i}$	Average oil velocity in duct i (m/s).
$\bar{v}_{in}$	Average pass-inlet oil velocity (m/s).
W_{plate}	Plate horizontal width (m).
W_{duct}	Vertical duct width (m).
α	Dimensionless horizontal duct height (H_{duct}/W_{duct}).
β	Dimensionless plate axial height (H_{plate}/W_{duct}).
β_T	Volumetric thermal expansion coefficient.
γ	Dimensionless plate radial width (W_{plate}/W_{duct}).
ρ	Oil density (kg/m^3).
μ	Oil dynamic viscosity ($Pa \cdot s$).

I. INTRODUCTION

THE oil flow distribution in a disc-type transformer winding has a direct impact on the cooling performance which, in conjunction with power loss distribution, determines the position and magnitude of the hot-spot temperature in the winding. In addition, the static pressure drop over a disc-type transformer winding determines the selection of pump for oil forced and directed (OD) cooling modes and more importantly oil split among windings connected hydraulically in parallel, for example LV winding and HV winding in the same phase.

Different models have been developed to predict oil flow distribution in and pressure drop over disc type transformer windings. These models can be grouped into two categories: network models [1]–[4] and computational fluid dynamics (CFD) models [5]–[7]. These two types of model share the same physical principles of conservation of mass, momentum and energy. Endeavors of combining the merits of both methods have been made by using CFD results to calibrate the correlation equations used in network models [8]–[10]. CFD modelling is usually conducted in axisymmetric 2D geometries to reduce computational requirements. Compared to 3D CFD

Manuscript received April 11, 2017; revised July 4, 2017; accepted August 3, 2017. Date of publication September 28, 2017; date of current version May 9, 2018. Paper no. TPWRD-00515-2017. *(Corresponding author: Zhongdong Wang.)*

X. Zhang, M. Daghrah, Z. Wang, and Q. Liu are with the School of Electrical and Electronic Engineering, The University of Manchester, Manchester M13 9PL, U.K. (e-mail: xiang.zhang-2@postgrad.manchester.ac.uk; muhammad.daghrah@postgrad.manchester.ac.uk; zhongdong.wang@manchester.ac.uk; qiang.liu@manchester.ac.uk).

P. Jarman is with the National Grid, Warwick, CV34 6DA, U.K. (e-mail: paul.jarman@uk.ngrid.com)

M. Negro is with Weidmann Electrical Technology AG, Chiasso 6830, Switzerland (e-mail: massimo.negro@wicor.com).

Color versions of one or more of the figures in this paper are available online at http://ieeexplore.ieee.org.

Digital Object Identifier 10.1109/TPWRD.2017.2739483

simulations, 2D simulations cannot capture detailed fluid flow and heat transfer phenomena in the vicinity of the spacers. However, for an ON cooling mode, comparisons of fluid flow and temperature distributions between 2D axisymmetric and 3D CFD models show that 2D results are representative of the 3D results as long as the governing dimensionless parameters (Gr/Re^2) are matched [7]. In addition, key 3D results, e.g., hot-spot temperature, can be derived from 2D CFD results based on the improvement strategies proposed in [7].

Only a few experimental studies were reported to record flow rates within horizontal cooling ducts to verify simulation models. Hot wire anemometry was used in [11] to record flow distribution within an isothermal winding model. It was observed that the lowest flow rate occurred in the central ducts of the tested pass of the winding model and more uniform flow distribution was achieved with wider inlet vertical cooling duct. A CCD camera was used in [12] to track the movements of tracer particles within a zig-zag disc type winding model under isothermal conditions. Pressure drops were measured along winding vertical ducts. It was observed in [12] that flow distribution is more uniform for lower number of discs per pass at the cost of higher pressure losses over the winding model. Reverse flow was observed in the first horizontal cooling duct under higher number of discs per pass. It was also reported in [12] that wider vertical ducts would produce more uniform flow distribution in and lower pressure drop over the winding. Laser doppler velocimetry was used to measure flow velocities within vertical cooling ducts in [13] to verify a proposed numerical model on a non-directed winding under nonisothermal conditions. Pressure drop over one pass of a winding model was measured in [14] to verify a 2D CFD model and a network model with calibrated correlation equations from [9].

Systematic simulation studies of oil flow distribution in and pressure drop over disc-type transformer windings were conducted by adopting dimensional analyses in [15]. From dimensional analyses, oil flow distribution and pressure drop were transformed to dimensionless parameters of flow proportion in each horizontal cooling duct and pressure drop coefficient over the winding, respectively. The controlling parameters were transformed to the Reynolds number at the winding pass inlet and dimensionless geometrical parameters (α, β, γ in [15]). The quantitative relationships between flow proportion, or pressure drop coefficient, and the dimensionless controlling parameters were obtained by conducting CFD parametric sweeps and correlating the CFD results with the controlling dimensionless parameters.

In this paper, experiments are designed to verify the method of dimensional analysis and the correlations obtained from CFD parametric sweeps. The experimental set-up and the implementation of the measurements of flow distribution and pressure drop are illustrated in Section II. Theoretical analyses and numerical modeling of the flow distribution in and pressure drop over the winding model are presented in Section III. In Section IV, experimental verification of the modeling results are presented. Finally, the comparisons of isothermal and nonisothermal measurements are shown in Section V, followed by discussion and conclusion in Sections VI and VII, respectively.

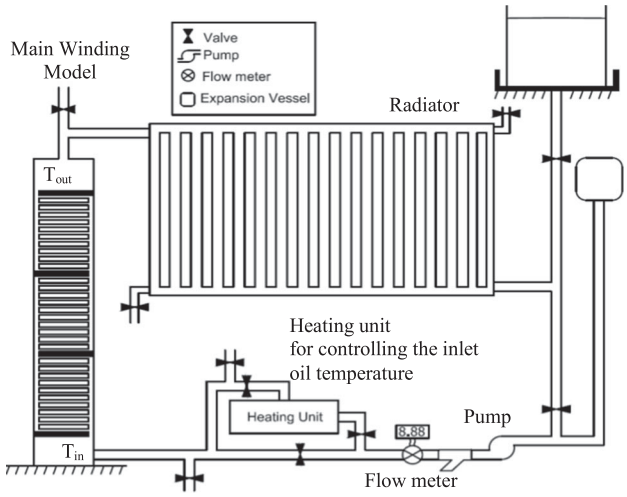

Fig. 1. Schematic diagram of the experimental setup.

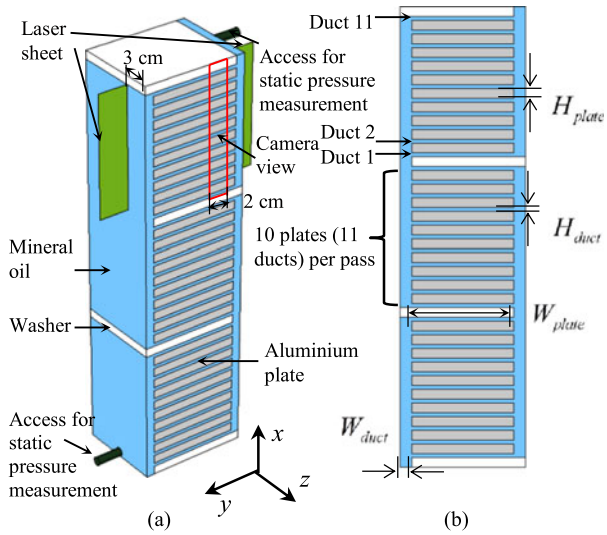

Fig. 2. Geometry of the winding model. (a) 3D geometry; (b) 2D geometry

II. Experimental Set-Up

Experimental setup is shown in Fig. 1. It consists of a winding model resembling a disc-type winding structure as shown in Fig. 2, a radiator to cool oil down, a pump to circulate oil and a flow meter to record flow rates. An external heating unit is used to heat up and control winding inlet oil temperature. The experimental setup is described as follows:

A. Winding Model

The rectangular winding model consists of 3 passes. Each pass is fitted with 10 disc segments. The disc segments are modeled as rectangular aluminum plates with geometrical dimensions of 100 mm × 104 mm × 10 mm. Each plate sits on 3 mm grooves of the side walls of the winding model making the actual depth of horizontal cooling ducts 94 mm. The winding model walls are made of lexan* 9030 polycarbonate sheets. Washers are made of acrylic material with geometrical

TABLE I
WIDING MODEL GEOMETRICAL PARAMETERS

Horizontal Duct depth	Horizontal duct height (H_{duct})	Vertical duct width (W_{duct})	Aluminum plates	
			Height (H_{plate})	Width (W_{plate})
94 mm	4 mm, 6 mm	10 mm, 12 mm	10 mm	104 mm

dimensions of 100 mm × (104 + vertical duct width) mm × 10 mm. Table I provides a summary of the geometrical dimensions of the winding models. Inner and outer vertical duct width are made equal and two vertical duct widths, 10 mm and 12 mm, are tested. The heights of horizontal ducts are uniform being 4 mm or 6 mm. Thermocouples are fitted at the inlet and outlet of the winding model to record winding inlet and outlet oil temperatures, respectively. Accuracy of the thermocouples used is ±1 °C.

The oil flow in the winding model is directed into a zigzag fashion using washers. Washers are placed at the entrance and exit of each pass. A washer blocks a vertical duct from one side and allows the oil to flow into or out of a pass from the opposite side. To guarantee complete oil blockage, silicone sealant is applied between a washer and the winding model wall at the location where the oil is desired to be blocked. It is intended that all plates and washers are perfectly aligned. However, during winding model assembly minimal geometrical deviations still occur, e.g., a plate is either slightly inward or outward. It was observed, after conducting the tests, that this slight geometrical deviation gives a signature, or a footprint, to the flow distribution within the pass as will be highlighted later. More details of the winding model can be found in [16].

B. Pressure Measurement

Two pressure ports, as shown in Fig. 2, were used to record static pressure drop over the 3-pass winding model with a differential pressure instrument. The pressure instrument has an accuracy of ±0.2% of the full scale of 10 kPa or equivalently the accuracy is ±20 Pa and a repeatability of ±10 Pa in this range. Each pressure measurement was taken 10 times. Since the pressure readings were stable, the average of the 10 measurements was used as a representative value.

C. Flow Measurement

Total oil flow rate is measured using a positive displacement flow meter, as it is less affected by viscosity variations, with accuracy of 0.5% of its reading. Within horizontal cooling ducts, a Particle Image Velocimetry (PIV) system is used to record oil flow rates. The PIV system consists of a laser source, light sheet optics and a camera. A synchronizer is used to synchronize the laser, the camera and the acquisition computer in order to obtain the velocity profile.

The accuracy of PIV measurements depends on the quality of the raw images photographed which is affected by both the density of seeding particles and their distribution within the duct. Silver coated hollow glass spheres with 9–14 micrometer diameter were used as seeding particles. In all PIV measurements, the laser sheet plane was aligned with the flow direction and perpendicular to the winding plate in each duct and was fixed only at one plane that is 3 cm from the winding model wall close to the camera. The camera field of view was focused on the 2 cm of the horizontal duct towards its exit as indicated in Fig. 2. PIV measurements were taken in steady state and in a hydraulically developed region in horizontal ducts. Twenty raw images were taken for each measurement and the statistical average of these images was used to extract the final result. The reason for using 20 raw images rather than using more is that a sweep of the number of raw images processed—1, 5, 10, 20, 30, 40, 50—shows that the case using 20 raw images gives results that are as accurate as those obtained from cases of larger number of images. More detailed description of the application of PIV to record oil flow rates in radial cooling ducts is given in [17]. Finally, the accuracy of PIV measurements was checked by comparing the total flow rate obtained from all the PIV measurements in pass 3 to that recorded by the flow meter. Discrepancies between the PIV results and the flow meter readings were within 7%.

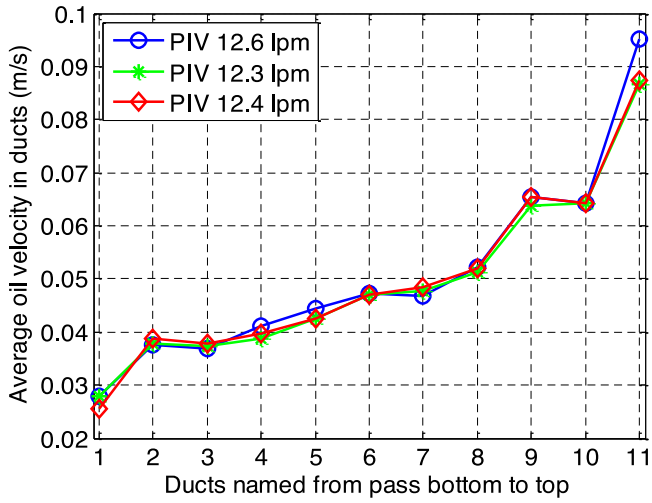

Fig. 3. Repeatability tests of the PIV system. In each test, total oil flow rate is controlled to be 12 lpm according to the reading of the flow meter and the sum of flow rate in each duct from PIV differs slightly from 12 lpm.

Flow distribution in a pass is hardly affected by the number of passes in the winding [15]. Therefore, only the flow rates within the horizontal cooling ducts of the third pass were measured using the PIV system. Fig. 3 shows the results of a experiment repeated 3 times in 3 different days, under the same operating conditions, to confirm the repeatability of the PIV measurements. In the repeatability tests, the total flow rate, recorded by the flow meter, was 12.0 litres per minute (lpm) while the inlet oil temperature was maintained within the range of 46 °C to 48 °C. It can be seen from Fig. 3 that the total flow rates derived from the PIV measurements are constantly slightly higher than that from the flow meter. This is partially because only one plane in the horizontal duct is measured and the end-wall effects are neglected.

D. Oil Properties

The tested oil is a mineral oil of which the variations of density and dynamic viscosity with temperature in Kelvin are shown in (1) and (2). These equations are from least-square curve fittings of the measured data provided by the oil manufacturer.

$$\rho = -0.65683 \times T + 1063.6 \tag{1}$$

$$\mu = 7.8630 \times 10^{-5} \times \exp\left(\frac{631.96}{T - 176.03}\right) \tag{2}$$

III. Analytical Analyses on Flow Distribution and Pressure Drop for the Winding Model

The methodology of conducting dimensional analyses, performing CFD parametric sweeps and correlating the CFD results with the identified dimensionless parameters was detailed in our previous publication [15]. This paper follows the same methodology for the winding model tested.

A. Dimensional Analyses on Pressure Drop Over and Flow Distribution in the Winding Model

In dimensional forms, the average oil velocity in a horizontal cooling duct *i* ($\bar{v}_i$) and the pressure drop over the 3-pass winding model (ΔP) can be expressed as functions shown in (3) and (4):

$$\bar{v}_i = f_i(n_2, \bar{v}_{in}, \rho, \mu, H_{duct}, H_{plate}, W_{plate}, W_{duct}) \tag{3}$$

$$\Delta P = g(n_1, n_2, \bar{v}_{in}, \rho, \mu, H_{duct}, H_{plate}, W_{plate}, W_{duct}) \tag{4}$$

These dimensional forms can be transformed to their dimensionless forms by choosing pass inlet velocity ($\bar{v}_{in}$), oil density (ρ), and vertical duct width (W_{duct}) as the repeating parameters. The dimensionless forms are (5) and (6):

$$\frac{\bar{v}_i}{\bar{v}_{in}} \cdot \frac{H_{duct}}{W_{duct}} = P_{fi} = f_i'(n_2, \mathrm{Re}, \alpha, \beta, \gamma) \tag{5}$$

$$\frac{\Delta P}{\rho \bar{v}_{in}^2/2} = C_{pd} = g'(n_1, n_2, \mathrm{Re}, \alpha, \beta, \gamma) \tag{6}$$

B. Parametric Sweeps

In the winding model, the number of discs per pass and the number of passes are 10 and 3, respectively, as shown in Fig. 2. In such a case, flow proportion in a duct *i* (P_{fi}) and pressure drop coefficient over the 3-pass winding model (C_{pd}) are functions of four dimensionless parameters: Re, α, $\beta$and γ.

According to the practical ranges of the total oil flow rate and the geometrical dimensions of disc-type transformer windings [15], [17], the four dimensionless parameters are set to be in the ranges shown in Table II. All the combinations of these discrete parameters were simulated by CFD simulations using COMSOL Multiphysics 5.2. In total, 720 CFD simulations were conducted involving 80 winding geometries which is the number of combinations of α, β and γ. Mesh refinement studies were conducted to guarantee mesh-independent results following the same procedures as presented in [15].

TABLE II
Ranges of the Swept Dimensionless Parameters

Symbol	Discrete parameter value
Re	20, 50, 100, 200, 400, 600, 800, 1000, 1200
α	0.25, 0.3, 0.4, 0.5, 0.6
β	0.67, 1, 2, 3
γ	6, 10, 12, 15

Discrete values are used to cover the practical range of each parameter.

C. Correlations

The results of flow proportion in the third pass and pressure drop coefficient over the 3-pass winding model were extracted and correlated with the four dimensionless controlling parameters by a multi-layer least square curve fitting strategy.

1) Correlation of Flow Distribution: The volumetric flow proportion in duct i in the third pass (P_{fi}) were correlated with Re, α, β and γ by equation set (7):

$$\begin{cases} P_{fi} = \frac{a_{i1}}{\mathrm{Re}^{1/3}} + a_{i2}\ln \mathrm{Re} + a_{i3}\mathrm{Re}^{1/3} + a_{i4}; \\ \qquad i = \{1, 2, \cdots, 11\} \\ a_{ij} = b_{ij1}\alpha^3 + b_{ij2}\alpha^2 + b_{ij3}\alpha + b_{ij4}; j = \{1, 2, 3, 4\} \\ b_{ijk} = c_{ijk1}\beta^3 + c_{ijk2}\beta^2 + c_{ijk3}\beta + c_{ijk4}; k = \{1, 2, 3, 4\} \\ c_{ijkm} = d_{ijkm1}\gamma^3 + d_{ijkm2}\gamma^2 + d_{ijkm3}\gamma + d_{ijkm4}; \\ \qquad m = \{1, 2, 3, 4\} \end{cases} \tag{7}$$

where $a_{ij}, b_{ijk}, c_{ijkm}$ are dummy correlation coefficients, which are determined from α, β, γ and the 256 coefficient $d's$ from the last equation in (7).

2) Correlation of Pressure Drop Coefficient: The pressure drop coefficient over the 3-pass winding model (C_{pd}) were correlated with Re, α, β and γ by equation set (8):

$$\begin{cases} C_{pd} = a_1 \frac{1000}{\mathrm{Re}} e^{a_2 \mathrm{Re}/1000} \\ a_i = b_{i1}(4\alpha)^{b_{i2}} e^{4\alpha b_{i3}}; \quad i = \{1, 2\} \\ b_{ij} = c_{ij1}\beta^{c_{ij2}} e^{c_{ij3}\beta}; \quad j = \{1, 2, 3\} \\ c_{ijk} = d_{ijk1}\gamma^3 + d_{ijk2}\gamma^2 + d_{ijk3}\gamma + d_{ijk4}; k = \{1, 2, 3\} \end{cases} \tag{8}$$

where a_i, b_{ij}, c_{ijk} are dummy correlation coefficients, which are determined from α, β, γ and the 72 coefficient $d's$ from the last equation in (8).

The aforementioned dimensional analyses offer ways to reduce the relationships between flow distribution, or pressure drop, and the controlling parameters to the simplest forms as expressed by (5) and (6). The CFD parametric sweeps and the subsequent correlations of the CFD results quantify the relationships as shown in (7) and (8).

IV. Experimental Verification of Dimensional Analyses and CFD Correlations

From the dimensional analyses presented in Section III, oil flow proportion in a duct and pressure drop coefficient over the

TABLE III
THREE CASES WITH SIMILAR RE

	Case 1	Case 2	Case 3
Pass inlet oil flow rate (lpm)	6	12	18
Oil temperature (°C)	77	48	36
Re (W_{duct} = 10 mm)	541	536	547
Re (W_{duct} = 12 mm)	531	526	537

TABLE IV
COMPARISON OF PRESSURE DROP AND PRESSURE DROP COEFFICIENT

		Case 1	Case 2	Case 3
10 mm	ΔP (pa)	43	200	466
	C_{pd}	9.1	10.4	10.6
12 mm	ΔP (pa)	37	148	303
	C_{pd}	11.29	11.04	9.96

3-pass winding model are functions of the Reynolds number at the winding inlet, α, β and γ. To validate the method of dimensional analysis and the correlations obtained, measurements of flow distribution in and pressure drop over the winding model were implemented and compared with the theoretical predictions from (7) and (8).

The experimental tests of the winding model were designed to fulfil two objectives:

1) To verify that P_{fi} and C_{pd} are controlled by *Re* itself instead of the components it is composed of.
2) To verify that results from the correlation equation sets (7) and (8) fit well with measurements in the practical range of *Re* for two chosen winding geometries: vertical duct width 10 mm and vertical duct width 12 mm.

Since vertical duct width is the denominator of the three dimensionless geometrical parameters, even the other geometrical dimensions keep unchanged each vertical duct width would lead to a new set of α, β and γ.

A. *Verification of Objective 1*

Since the hydraulic diameter is defined as $D_h = 4\,A/P$, for a given oil type, the Reynolds number at the winding pass inlet is mainly controlled by the total oil flow rate and the oil temperature. The tested three cases with similar *Re* for two vertical duct widths 10 mm and 12 mm are shown in Table III.

1) Flow Distribution: For the winding model of vertical duct width 10 mm, the comparisons of average oil velocities and flow proportions in the third pass from PIV measurements are shown in Fig. 4(a) and (b), respectively. The comparisons for vertical duct width 12 mm are shown in Fig. 5. It can be seen from both Figs. 4 and 5 that although the average velocities for the three cases are different, the flow distributions in terms of volumetric flow proportion in each duct are almost identical.

2) Pressure Drop Coefficient: The comparisons of pressure drops and pressure drop coefficients over the 3-pass winding model for vertical duct width 10 mm and 12 mm are shown in Table IV. For each geometry, the absolute static pressure

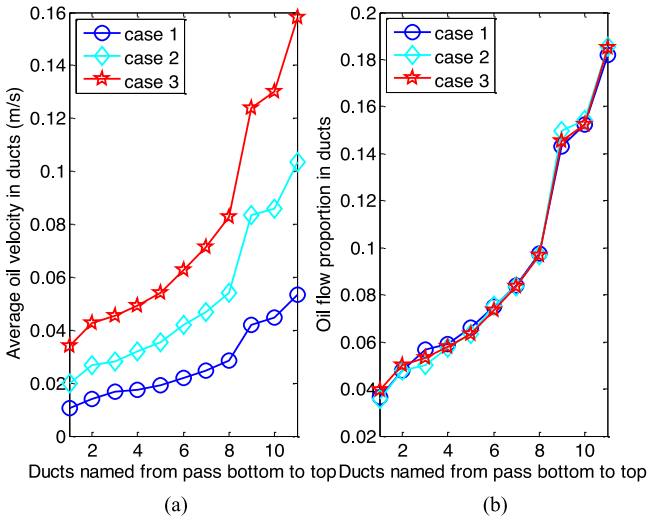

Fig. 4. Comparison of flow distribution for the three cases in Table III with similar *Re* and vertical duct width of 10 mm. (a) Average velocity. (b) Flow proportion where the total oil flow rate is regarded as one unit.

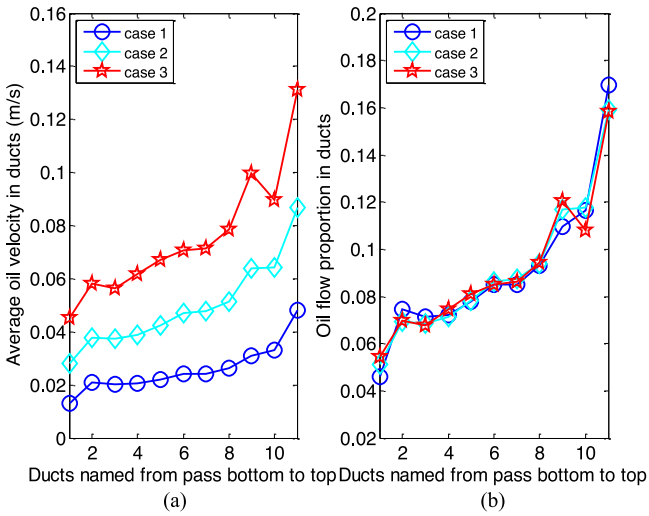

Fig. 5. Comparison of flow distribution for the three cases in Table III with similar *Re* and vertical duct width of 12 mm. (a) Average velocity. (b) Flow proportion where the total oil flow rate is regarded as one unit.

drops are very different but the corresponding pressure drop coefficients are similar.

From these comparisons for flow distributions and pressure drop coefficients from cases with similar Re, objective 1 is acceptably achieved.

B. *Verification of Objective 2*

1) Flow Distribution: To verify that the flow distribution correlation equation set (7) holds valid in the practical range of Re, flow distributions of two more cases were tested for both geometries. The tested cases are shown in Table V.

For the geometry of vertical duct width 10 mm, the comparisons of average oil velocities and flow proportions obtained from PIV measurements and (7) are shown in Fig. 6(a) and (b), respectively. The comparisons for vertical duct width 12 mm

TABLE V
THREE CASES TO COVER THE PRACTICAL RANGE OF RE

	Case 4	Case 2	Case 5
Pass inlet oil flow rate (lpm)	6	12	18
Oil temperature (°C)	20	48	70
Re (W_{duct} = 10 mm)	97	536	1402
Re (W_{duct} = 12 mm)	95	526	1375

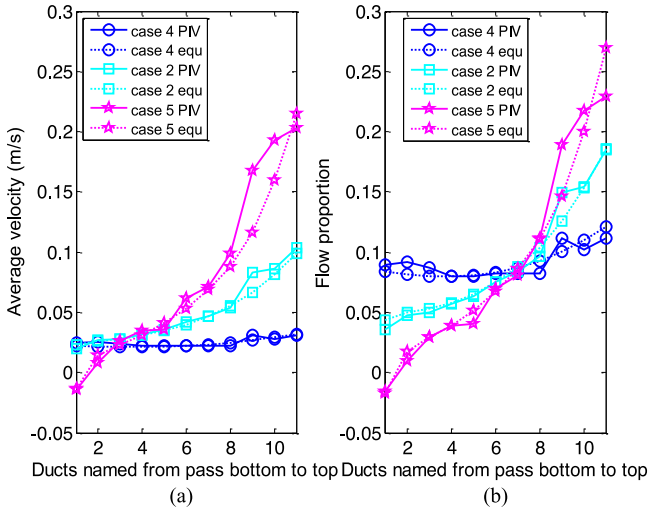

Fig. 6. Comparison of flow distribution for *Re* in the range in Table VI with vertical duct width being 10 mm. (a) Average velocity in each duct of pass 3. (b) Flow proportion in each duct of pass 3 where the total oil flow rate is regarded as one unit. The legend 'equ' refers to correlation (7).

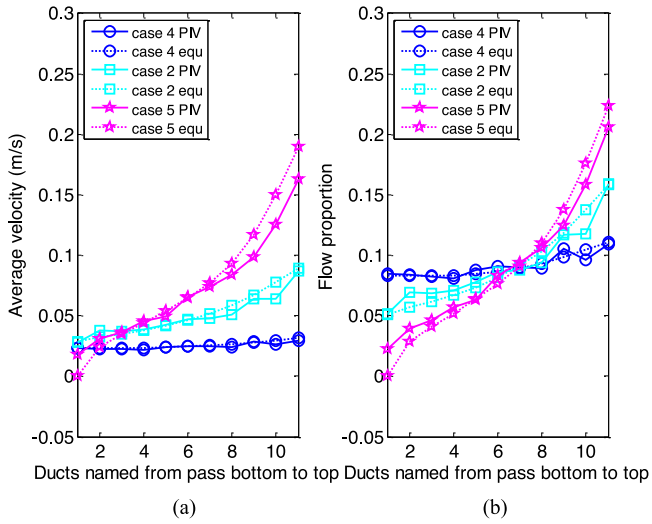

Fig. 7. Comparison of flow distribution for *Re* in the range in Table VI with vertical duct width of 12 mm. (a) Average velocity in each duct of pass 3. (b) Flow proportion in each duct of pass 3 where the total oil flow rate is regarded as one unit. The legend 'equ' refers to correlation (7).

TABLE VI
TEST CONDITIONS OF VASE 6 AND CASE 7

	Case 6	Case 7
Pass inlet oil flow rate (lpm)	12	12
Oil temperature (°C)	70	70
Vertical duct width (mm)	10	10
Horizontal duct height (mm)	4	6
α	0.4	0.6
Re	878	878

are shown in Fig. 7. As can be seen from both Figs. 6 and 7, results from both methods share the same varying trends. With the increase of Re, flow distribution gets less uniform.

For case 4 and case 2, flow distribution curves from the equation set (7) follow closely the PIV results for both geometries. For case 5, the flow distribution curves from the two methods deviate more from each other.

For case 5 of the 10 mm vertical duct width geometry, both PIV measurement and the flow correlation equation set (7) show the occurrence of reverse flow at the bottom of the pass; for the geometry of vertical duct width 12 mm, the correlation shows a nearly stagnated flow in the horizontal duct at the bottom of the pass, while the PIV measurement shows an average velocity of 18 mm/s. Apart from the difference in total oil flow rate obtained from PIV measurements and that from the flow meter, which is the input for (7), and the geometrical deviations of the winding model as is mentioned in Section II part A, another reason for the increased discrepancy could be that *Re* for case 5 (around 1400) is beyond the upper boundary of *Re* (*Re* = 1200) in the CFD parametric sweeps from which the correlation equation sets were derived. It is worth mentioning that case 5 should be avoided in real transformers because the occurrence of reverse flow can seriously jeopardize the cooling performance.

Comparing Figs. 6 and 7, we can see that with the increase of vertical duct width (mainly due to the decrease of α) oil flow distribution gets relatively more uniform. To further verify the point that the decrease of α brings a relatively more uniform flow distribution, a comparison between two cases with different horizontal duct heights is executed. The test conditions of the two cases are shown in Table VI and the comparison of flow distribution is shown in Fig. 8. As can be seen from Fig. 8, the flow distribution for the case of α being 0.4 is more uniform than the case of α being 0.6. In fact, reverse flow occurs for the case of α being 0.6. In addition, the predicted results obtained from (7) follow the measured results closely. The velocity profiles in the bottom ducts of case 6 and case 7 are shown in Fig. 9. Half of the PIV images and velocity profiles are shown in Fig. 9 because they are symmetric to the central axes. The velocity of the reversed flow in case 7 is designated as negative velocities.

2) Pressure Drop Coefficient: To verify that the pressure drop coefficient correlation equation set (8) holds valid in the practical range of Re, more pressure measurements were implemented. In these measurements, oil temperature was set to be 20 °C, 35 °C, 50 °C, and 77 °C while the total oil flow rates ranges from 6 lpm to 18 lpm for the vertical duct width 10 mm geometry and 6 lpm to 21 lpm for the geometry of vertical duct width 12 mm. For the geometry of vertical duct width 10 mm, the comparisons of pressure drops and pressure drop coefficients obtained from the measurements and (8) are shown in Fig. 10(a) and (b), respectively. The comparisons for vertical

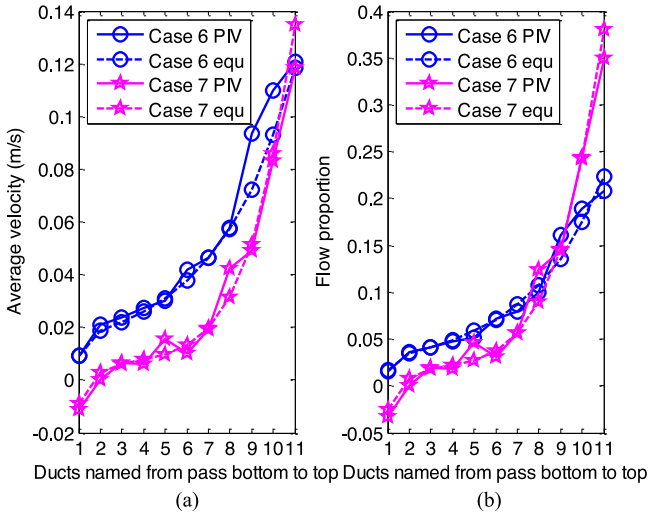

Fig. 8. Comparison of flow distribution for two horizontal duct heights in Table VI. (a) Average velocity in each duct of pass 3 where the total oil flow rate is regarded as one unit. (b) Flow proportion in each duct of pass 3. The legend 'equ' refers to correlation (7).

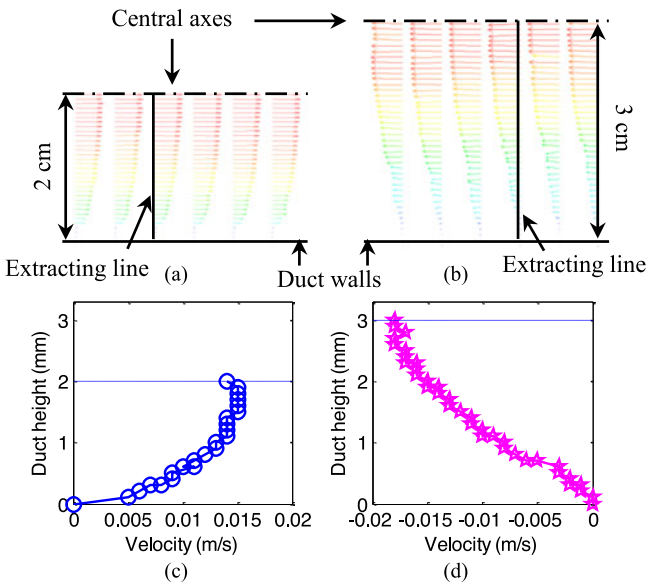

Fig. 9. Velocity profiles in the first ducts of case 6 and case 7 from PIV measurements. (a) Half of the processed PIV image for case 6. (b) Half of the processed PIV image for case 7. (c) Velocity profile on the extracting line for case 6. (c) Velocity profile on the extracting line for case 7.

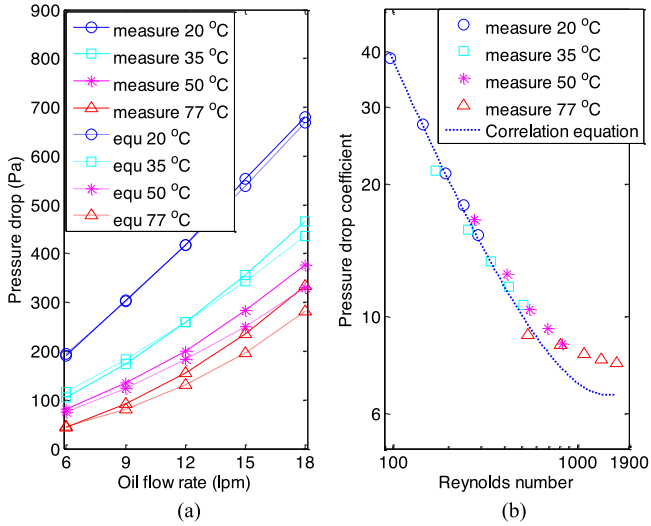

Fig. 10. Comparison of static pressure drops for the geometry of vertical duct width being 10 mm. (a) absolute pressure drop; (b) pressure drop coefficient.

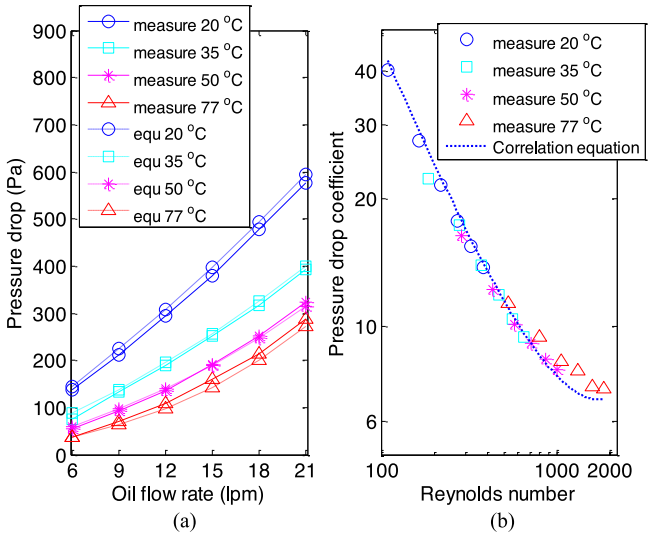

Fig. 11. Comparison of static pressure drops for the geometry of vertical duct width of 12 mm. (a) absolute pressure drop; (b) pressure drop coefficient

duct width 12 mm are shown in Fig. 11. As can be seen from both Figs. 10 and 11, the pressure drops from measurements and those derived from (8) are consistent with maximum relative error being 16.9%. From the prediction of (8), the variation of pressure drop coefficient against *Re* for both geometries in log-log scale is a straight line at the beginning and then levels off in the region of high Re. When the measured pressure points are transformed to pressure drop coefficients, they fall close to the predicted curves from (8) and in the same way with maximum relative error being 16.9%.

From the comparisons for flow distributions and pressure drops from cases covering the practical range of Re, objective 2 is acceptably achieved.

V. Comparison of Isothermal and Nonisothermal Cases

In practice, buoyancy force and hot-streak dynamics are involved in determining flow distribution in and pressure drop over the winding, especially for oil natural (ON) cooling modes [5]–[7]. To verify that for OD cooling modes the influences of buoyancy force and hot-streak dynamics are negligible and therefore the foregoing isothermal results hold valid for practical cases, comparison between isothermal and nonisothermal cases are shown in this section.

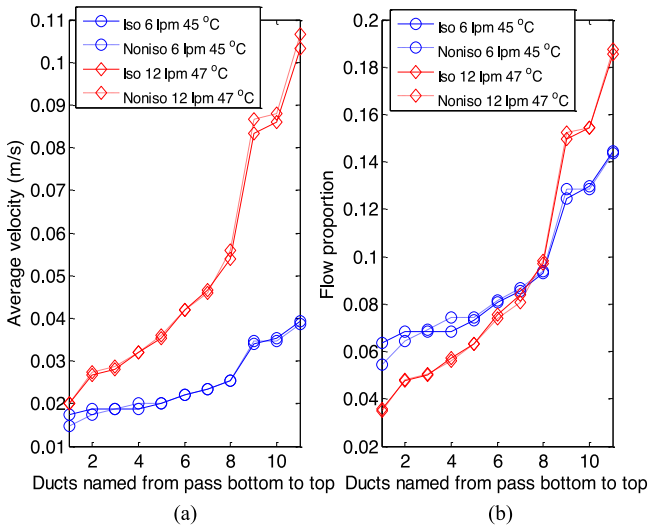

Fig. 12. Comparison of flow distribution for isothermal and nonisothermal flow conditions with vertical duct width being 10 mm. (a) average velocity in each duct; (b) flow proportion in each duct where the total oil flow rate is regarded as one unit.

TABLE VII
PARAMETERS RELATED TO NONISOTHERMAL TESTS

	6 lpm	12 lpm
Pass 3 inlet temperature (°C)	45	47
Pass 3 outlet temperature (°C)	48	48.5
Ri (Gr/Re^2)	0.046	0.006

The thermal expansion coefficient is 7.8×10^{-4} [1/K] and the temperature gradients in the definition of *Ri (Gr/Re^2)* are taken as the differences between pass 3 outlet temperatures and pass 3 inlet temperatures.

A. Power Injection in Each Plate

The current density in the copper conductor of a disc-type power transformer is in the range of 2–4 A/mm^2 [19]. Assuming the plates in the winding model were made of copper and a current density of 4 A/mm^2 ran through each plate with copper resistance at 85 °C, then the resistive power generated in each plate would be approximately 35 W. To account stray losses and eddy current losses in the winding and to provide some margin, a power injection of 50 W per plate was selected which was delivered by two cartridge heaters embedded in each plate as detailed in [16].

B. Comparisons of Flow Distribution and Pressure Drop

The comparisons of flow distribution and pressure drop between isothermal and nonisothermal conditions were implemented on the winding geometry of vertical duct width 10 mm. For an OD cooling mode, typical oil velocity in horizontal ducts range from 0.075 m/s to 0.15 m/s [18]. Therefore, oil velocity at the winding pass inlet would be larger than 0.1 m/s corresponding to a total oil flow rate of approximately 6 lpm. In the nonisothermal tests, two flow rates of 6 lpm and 12 lpm are tested, of which the related parameters are shown in Table VII.

TABLE VIII
COMPARISON OF PRESSURE DROP AND PRESSURE DROP COEFFICIENT

		6 lpm 45 °C	12 lpm 47 °C
Isothermal	ΔP (pa)	91	223
Nonisothermal	ΔP (pa)	90	215

Each pressure drop result is the average of ten repeated tests.

For comparison purposes, two isothermal flow cases of 6 lpm, 45 °C and 12 lpm, 47 °C were conducted.

The comparisons of flow distributions in pass 3 from PIV measurements are shown in Fig. 12. As can be seen, flow distributions from isothermal and nonisothermal conditions are almost identical. The comparisons of pressure drops for these isothermal and nonisothermal cases are shown in TableVIII. The discrepancies on pressure drop between the isothermal and nonisothermal cases are negligible. The negligible *Ri's* (*Gr/Re^2*) for case 6 and case 7 (much smaller than 1) shown in Table VII is responsible for the negligible differences in flow and pressure drop results between the isothermal and nonisothermal cases.

It can be concluded that for OD cooling modes, the influences of buoyancy force and hot-streak dynamics are negligible. Therefore, the aforementioned results obtained from isothermal flow conditions are valid for OD cooling modes.

VI. DISCUSSION

The method of dimensional analysis, which can simplify a physical problem to its simplest form prior to obtaining a quantitative relationship, has been widely used in fluid mechanics. However, it has not yet become the common practice for transformer thermal modeling.

In this paper, the methodology presented in [15] was verified experimentally on disc-type transformer winding models. It is worth emphasizing that none of the experimental scenarios were simulated directly by CFD, yet the experimental results are in line with the results generated from the correlation equation sets obtained from 2D CFD parametric sweeps. Therefore the 2D modeling, the method of dimensional analysis, the CFD simulations, and the correlations of the CFD results are all verified to be valid for the investigation of flow distribution and pressure drop. In addition, comparisons between several typical experimental tests and CFD simulations of the same conditions were also made, of which the fluid flow and pressure drop results from the CFD simulations and experimental tests were as consistent as those generated from the correlation equation sets.

Since the correlation equation sets have been verified experimentally, some insight into oil flow distribution in and pressure drop over the winding model can be obtained conveniently from the correlation equation sets. It was found that the geometrical parameter α is more influential than the other two geometrical parameters β and γ [15].

The uniformity of oil flow distribution in a pass can be represented by a parameter called maldistribution defined as the ratio of the maximum to the minimum flow rate in the ducts of a pass [10]. For the 3-pass winding model with 10 plates per

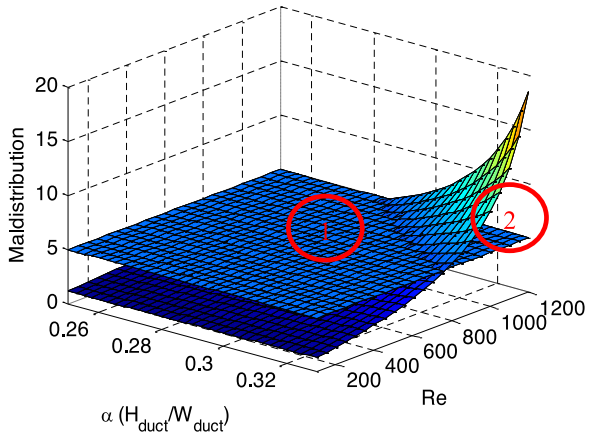

Fig. 13. Variation of maldistribution with *Re* and α. In region 1, maldistribution is smaller than 5, whereas in region 2 maldistribution is larger than 5.

pass (11 ducts), with the help of the flow correlation equation set (7), the variation of maldistribution with the two influential parameters, *Re* and α, can be obtained conveniently with β set to be 1 (vertical duct width equals disc axial height) and γ to be 10 (disc radial width is 10 times vertical duct width), as shown in Fig. 13. It can be seen that maldistribution increases monotonically with increasing *Re* and α. The higher the total oil flow rate and the larger the ratio of horizontal duct height to vertical duct width, the more distorted the flow distribution would be. For design purpose, if maldistribution is desired to be smaller than 5, then region 1 indicates the feasible combinations of *Re* and α, as shown in Fig. 13.

It was observed in the experiments that geometrical deviations lead to non-smooth flow distribution which could cause some horizontal cooling ducts suffering from smaller flow rate than expected. Although the trend of flow distribution will not change significantly, the reduction of flow rate in some specific ducts may still cause noticeable winding temperature rise. Geometrical deviations during the transformer manufacturing process are difficult to avoid and therefore the effects of some typical geometrical deviations are worth further investigation.

VII. Conclusion

Dimensional analyses were conducted to simplify the physical problems of oil flow distribution in and pressure drop over a winding model to the simplest forms. CFD parametric sweeps of the identified dimensionless controlling parameters were performed and then the CFD results obtained were correlated to form predictive correlation equation sets.

Measurements of flow distribution in pass 3 using a PIV system and recording of pressure drop over the 3-pass winding model were implemented to verify the method of dimensional analysis and the correlation equation sets obtained from CFD parametric sweeps. The fact that it is the Reynolds number itself instead of the way how it is composed of that controls oil flow distribution and pressure drop coefficient, was verified experimentally for a fixed winding geometry in OD cooling modes.

It was also satisfactorily verified that the correlation equation sets can generate results that are in line with the measurements in the practical range of Re. Therefore, the 2D CFD simulations and the strategies of correlating the CFD results to form predictive correlation equation sets are also valid. The application of the correlations to real 3D cylindrical windings needs further validation.

The conclusions on flow distribution in and pressure drop over the winding obtained from isothermal conditions can be extended to nonisothermal conditions in OD cooling modes, as the experiments on nonisothermal conditions confirmed that the effects of buoyancy force and hot-streak dynamics over flow distribution and pressure drop are negligible for the tested OD conditions. However, the effects of buoyancy forces and hot-streak dynamics on heat transfer in the winding need further investigation.

Acknowledgment

The authors would like to express their gratitude to M&I Materials, National Grid, Scottish Power, Shell, TJ|H2b Analytical Services, U.K. Power Networks and Weidmann Electrical Technology AG for their financial and technical contributions to the Transformer Research Consortium at The University of Manchester.

References

[1] A. J. Oliver, "Estimation of transformer winding temperatures and coolant flows using a general network method," *Proc. Inst. Elect. Eng.*, vol. 127, pp. 395–405, Nov. 1980.

[2] Z. R. Radakovic and M. S. Sorgic, "Basics of detailed thermal-hydraulic model for thermal design of oil power transformers," *IEEE Trans. Power Del.*, vol. 25, no. 2, pp. 790–802, Apr. 2010.

[3] E. Rahimpour, M. Barati, and M. Schäfer, "An investigation of parameters affecting the temperature rise in windings with zigzag cooling flow path," *Appl. Therm. Eng.*, vol. 27, no. 11, pp. 1923–1930, 2007.

[4] J. Zhang and X. Li, "Coolant flow distribution and pressure loss in ONAN transformer windings. Part I: Theory and model development," *IEEE Trans. Power Del.*, vol. 19, no. 1, pp. 186–193, Jan. 2004.

[5] F. Torriano, M. Chaaban, and P. Picher, "Numerical study of parameters affecting the temperature distribution in a disc-type transformer winding," *Appl. Therm. Eng.*, vol. 30, no. 14, pp. 2034–2044, 2010.

[6] A. Skillen, A. Revell, H. Iacovides, and W. Wu, "Numerical prediction of local hot-spot phenomena in transformer windings," *Appl. Thermal Eng.*, vol. 36, pp. 96–105, 2012.

[7] F. Torriano, P. Picher, and M. Chaaban, "Numerical investigation of 3D flow and thermal effects in a disc-type transformer winding," *Appl. Therm. Eng.*, vol. 40, pp. 121–131, 2012.

[8] W. Wu, Z.D. Wang, A. Revell, H. Iacovides, and P. Jarman, "Computational fluid dynamics calibration for network modelling of transformer cooling oil flows-part I heat transfer in oil ducts," *IET Elect. Power Appl.*, vol. 6, no. 1, pp. 19–27, 2012.

[9] W. Wu, Z.D. Wang, A. Revell, and P. Jarman, "Computational fluid dynamics calibration for network modelling of transformer cooling flows–Part II: Pressure loss at junction nodes," *IET Elect. Power Appl.*, vol. 6, no. 1, pp. 28–34, 2012.

[10] J. Coddé, W. Van der Veken, and M. Baelmans, "Assessment of a hydraulic network model for zig–zag cooled power transformer windings," *Appl. Therm. Eng.*, vol. 80, pp. 220–228, 2015.

[11] P. Allen, O. Szpiro, and E. Campero, "Thermal analysis of power transformer windings," *Elect. Mach. Electromech.*, vol. 6, no. 1, pp. 1–11, 1981.

[12] M. Nakadate, K. Toda, K. Sato, D. Biswas, C. Nakagawa, and T. Yanari, "Gas cooling performance in disc winding of large-capacity gas-insulated transformer," *IEEE Trans. Power Del.*, vol. 11, no. 2, pp. 903–908, Apr. 1996.

[13] J.-M. Mufuta, "Comparison of experimental values and numerical simulation on a set-up simulating the cross-section of a disc-type transformer," *Int. J. Therm. Sci.*, vol. 38, no. 5, pp. 424–435, 1999.
[14] A. Weinläder, W. Wu, S. Tenbohlen, and Z. D. Wang, "Prediction of the oil flow distribution in oil-immersed transformer windings by network modelling and computational fluid dynamics," *IET Elect. Power Appl.*, vol. 6, no. 2, pp. 82–90, 2012.
[15] X. Zhang, Z. D. Wang, and Q. Liu, "Prediction of Pressure drop and flow distribution in disc type transformer windings in an OD cooling mode," *IEEE Trans. Power Del.*, vol. 32, no. 4, pp. 1655–1664, Aug. 2017.
[16] M. Daghrah, Z. D. Wang, Q. Liu, D. Walker, P. W. R. Smith, and P. Mavrommatis, "Design of experimental setup to study factors affecting hot spot temperature in disc type winding transformers," in *Proc. IET Int. Conf. Resilience Transm. Distrib. Netw.*, Birmingham, UK, Sep. 2015.
[17] M. Daghrah, Z. D. Wang, Q. Liu, C. Krause, and P. W. R. Smith, "Characterization of oil flow rates within radial cooling ducts of disc type winding transformers using particle image velocimetry," *IEEE Elect. Insul. Mag.*, under review.
[18] J. Zhang and X. Li, "Coolant flow distribution and pressure loss in ONAN transformer windings. Part II: Optimization of design parameters," *IEEE Trans. Power Del.*, vol. 19, no. 1, pp. 194–199, Jan. 2004.
[19] M. Heathcote, *J & P Transformer Book*, 13th ed. Amsterdam, The Netherlands: Elsevier, 2007.

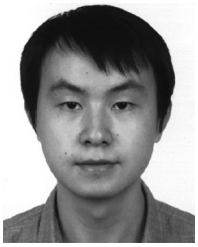

Xiang Zhang received the B.Eng. degree in electrical and electronic engineering from Xi'an Jiaotong University, Xi'an, China, in 2012. He is working toward the Ph.D. degree at the Electrical Energy and Power Systems Group, School of Electrical and Electronic Engineering, The University of Manchester, Manchester, U.K., since 2014 His research program is on transformer thermal modelling.

Muhammad Daghrah received the B.Eng. degree in electrical engineering from Birzeit University, Palestine, Birzeit, in 2010, where he worked for two years as a Teaching Assistant and the M.Sc. degree in electrical power systems engineering from The University of Manchester, Manchester, U.K., in 2013. He is currently studying as a Ph.D. student at The University of Manchester. His research interests include condition monitoring of power system assets.

Zhongdong Wang received the B.Sc. and M.Sc. degrees in high-voltage engineering from Tsinghua University, Beijing, China, in 1991 and 1993, and the Ph.D. degree in electrical engineering from The University of Manchester, Manchester, U.K., in 1999. She is currently a Professor of high-voltage engineering with the School of Electrical and Electronic Engineering, The University of Manchester. Her research interests focus on power transformers covering all aspects of modelling and simulation, materials and systems, and asset-management policies.

Qiang Liu (S'08-M'12) received the B.Eng. degree in electrical engineering and the M.Eng. degree in high voltage and electrical insulation from Xi'an Jiaotong University, Xi'an, China, in 2005 and 2008, respectively, and the Ph.D. degree in electrical power engineering from The University of Manchester, Manchester, U.K., in 2011. He is currently a Lecturer in the School of Electrical and Electronic Engineering, The University of Manchester. His research interests include prebreakdown and breakdown phenomena in liquids, ester transformer liquids, streaming electrification, aging of insulating materials, transformer asset management, and high-voltage testing.

Paul Jarman was born in London, U.K., on September 27, 1962. He received the Graduate degree from Cambridge University, Cambridge, U.K., in 1984 with an Honors degree in electrical science. He joined the Central Electricity Generating Board, Research Division, working on, amongst other projects, FRA testing of transformers. In 1990, he joined the National Grid as a transformer engineer, becoming head of transformers in 1998. Since 2001, he has been National Grid's technical specialist for transformers now within the Asset Management group. Mr. Jarman is Chairman of IEC TC14, the international committee for power transformer standards, U.K. regular member of CIGRE study committee A2 for transformers, and has recently been the convenor of a CIGRE group on transformer monitoring. He is a Chartered Electrical Engineer and member of the IET.

Massimo Negro received the M.S. degree in electrical engineering from the Universita degli Studi di Pavia, Pavia, Italy, in 1998. From 1997 to 2001, he was with Tamini Trasformatori S.r.l, Melegnano, Italy, as Electrical Designer of industrial transformer for high-current applications, such as arc furnace and rectifier transformers ($>$100 kA). From 2001 to 2003 he was with ABB Trasformatori S.p.A., Legnano, Italy, as Electrical Designer of Industrial and Power transformers ($>$100 kA and $>$400 kV, respectively). Since 2003, he has been with Weidmann Electrical Technology AG, Rapperswil, Switzerland, as Electrical Engineer, applying high current–high voltage transformer design reviews. His current research interests include 3-D electromagneto-thermal coupled and computed fluid dynamic finite-element simulations of high-current high-voltage transformer models. Mr. Negro is a member of the IEEE Electromagnetic Compatibility Society and the IEEE Magnetics Society and a member of IEC-CEI CT 14.